A dynamic loop in halohydrin dehalogenase HheG regulates activity and enantioselectivity in epoxide ring opening

Marcel Staar[a]+, Lina Ahlborn[a]+, Miquel Estévez-Gay[b], Katharina Pallasch[a], Sílvia Osuna*[b,c], Anett Schallmey*[a,d,e]

[a] M. Staar, L. Ahlborn, K. Pallasch, Prof. A. Schallmey
Institute for Biochemistry, Biotechnology and Bioinformatics, Technische Universität Braunschweig, Spielmannstr.7, 38106 Braunschweig (Germany)
[b] Dr. Miquel Estévez-Gay, Prof. Dr. Sílvia Osuna
CompBioLab Group, Institut de Química Computacional i Catàlisi (IQCC), Departament de Química, Universitat de Girona, c/Maria Aurèlia Capmany 69, 17003 Girona, Catalonia, Spain
[c] Prof. Dr. Sílvia Osuna
ICREA, Passeig Lluís Companys 23, 08010 Barcelona, Catalonia, Spain
[d] Prof. A. Schallmey
Zentrum für Pharmaverfahrenstechnik (PVZ), Technische Universität Braunschweig, Franz-Liszt-Str. 35a, 38106 Braunschweig (Germany)
[e] Prof. A. Schallmey
Braunschweig Integrated Center of Systems Biology (BRICS), Technische Universität Braunschweig, Rebenring 56, 38106 Braunschweig (Germany)

*Correspondence:
Prof. Dr. Anett Schallmey, Institute for Biochemistry, Biotechnology and Bioinformatics, Technical University Braunschweig, Spielmannstr. 7, 38106 Braunschweig, Germany.
E-mail: a.schallmey@tu-braunschweig.de

Prof. Dr. Sílvia Osuna, Institut de Química Computacional i Catàlisi (IQCC), Departament de Química, Universitat de Girona, c/Maria Aurèlia Capmany 69, 17003 Girona, Catalonia, Spain
E-mail: silviaosu@gmail.com

+ Both authors contributed equally to this work

ABSTRACT

Halohydrin dehalogenase HheG and its homologs are remarkable enzymes for the efficient ring opening of sterically demanding internal epoxides using a variety of nucleophiles. The enantioselectivity of respective wild-type enzymes, however, is usually insufficient for application and frequently requires improvement by protein engineering. We herein demonstrate that the highly flexible N-terminal loop of HheG, comprising residues 39 to 47, has a tremendous impact on the activity as well as enantioselectivity of this enzyme in the ring opening of structurally diverse epoxide substrates. Thus, highly active and enantioselective HheG variants could be accessed through targeted engineering of this loop. In this regard, variant M45F displayed almost 10-fold higher specific activity than wild type in the azidolysis of cyclohexene oxide, yielding the corresponding product (1S,2S)-2-azidocyclohexan-1-ol in 96%ee$_P$ (in comparison to 49%ee$_P$ for HheG wild type). Moreover, this variant was also improved regarding activity and enantioselectivity in the ring opening of cyclohexene oxide with other nucleophiles, demonstrating even inverted enantioselectivity with cyanide and cyanate. In contrast, a complete loop deletion yielded inactive enzyme. Concomitant computational analyses of HheG M45F in comparison to wild type enzyme revealed that mutation M45F promotes the productive binding of cyclohexene oxide and azide in the active site by establishing non-covalent C-H ⋅⋅π interactions between epoxide and F45. These interactions further position one of the two carbon atoms of the epoxide ring closer to the azide resulting in higher enantioselectivity. Additionally, stable and enantioselective cross-linked enzyme cystals of HheG M45F were successfully generated after combination with mutation D114C.

Keywords: *halohydrin dehalogenase, protein engineering, enantioselectivity, epoxide ring opening, molecular dynamics, cross-linked enzyme crystals*

INTRODUCTION

Enantioselectivity is often a major driver for application of enzyme-catalyzed reactions in chemical synthesis. Although a number of native enzymes have been described that generally display high to absolute enantioselectivity in their catalyzed reactions,[1–5] in the majority of cases the selectivity of an enzyme varies from substrate to substrate. For this reason, protein engineering is often vital to adjust the enantioselectivity of a native enzyme (along with other enzyme characteristics) to fulfill the requirements of an industrial biocatalytic process.[6–9]

Halohydrin dehalogenases (HHDHs) have gained increasing attention in recent years for their application in the synthesis of a plethora of valuable products.[10] Naturally, those enzymes catalyze the reversible dehalogenation of β-haloalcohols with formation of the corresponding epoxides.[11] In the reverse reaction, a range of small C-, O-, N- and S-nucleophiles, such as azide, cyanide, nitrite, cyanate and thiocyanate (known as pseudohalogens), are also accepted for epoxide ring opening in addition to halide ions (Figure 1A).[12] This enabled the preparation of enantioenriched β-nitroalcohols,[13] β-cyanohydrins,[14] oxazolidinones[15] and thiiranes[16] amongst others,[17–20] fueled by the recent discovery of many new HHDHs from public sequence databases.[13,21–24] In most of these cases, however, protein engineering of the initially identified enzymes with highest activity was still necessary to achieve also high enantioselectivity. Apart from a few examples,[13,25–29] most native HHDHs do not display high enantioselectivity as this would contradict their assumed natural function, which is presumably the detoxification and degradation of (naturally occurring) haloalcohols.[30,31]

Many examples for the protein engineering of selected HHDHs, such as HheC from *Agrobacterium radiobacter* AD1, have been reported in literature that do not only focus on enantioselectivity but also on activity and stability.[32–39] Of these examples, the majority profited from the previously solved crystal structures of respective enzymes. Thus, crystal structures for members of almost all currently known HHDH subtypes A-G have been reported by now.[13,40–44] One of them is HheG from *Ilumatobacter coccineus*.[42] This enzyme was the first reported HHDH displaying unexpectedly high activity on cyclic as well as other sterically demanding internal epoxide substrates, owing to its much broader and more solvent-exposed active site compared to other HHDHs.[42,45–47] Since its discovery in 2017, a few more G-type HHDHs have been characterized, all displaying similar substrate scopes as HheG.[13,47,48] Despite this appealing activity towards bulky epoxides, HheG as well as other G-type members also come with some limitations including their insufficient stability for industrial application as well as an only moderate enantioselectivity.[37,42,47] The first challenge, the poor (thermal) stability of HheG, was already addressed by us through protein engineering as well as immobilization.[37,49,50] Thus, we could demonstrate that the exchange of residue T123 in HheG by aromatic amino acids or glycine resulted in variants with up to 14 K higher apparent melting temperature as well as increased activity, most likely through regulating the dynamics of an N-terminal loop spanning residues 39-47 (Figure 1B).[37] Interestingly, a slight increase in the enantioselectivity of those HheG variants was observed as well. In a complementary approach to stabilize HheG for application, we recently prepared cross-linked enzyme crystals (CLECs) after crystal contact engineering of HheG to introduce defined cross-linking sites.[49,50] This yielded highly stable and reusable enzyme preparations with remarkable resistance towards temperature, pH and the presence of organic solvents. Moreover, some of the HheG mutants

3

generated during crystal contact engineering also displayed improved enantioselectivity.[49,50] This time, respective mutations (M45C and V46K) were directly located on the flexible *N*-terminal loop, opposite to the catalytic triad of HheG (Figure 1B). This loop can occur in an open as well as closed conformation (Figure 1B), as demonstrated by X-ray analysis and MD simulations, thus confining the active site and impacting substrate access.[37,51]

Very recently, also the first studies on the enantioselectivity engineering of HheG have been reported. These yielded HheG mutants with high enantioselectivity in the synthesis of chiral aryl- and spiro-oxazolidinones as well as the azidolysis of cyclohexene oxide and cyclopentene oxide.[52–55] In all cases, substrate docking based on the published crystal structure of HheG[42] was used to identify relevant residues within the enzyme active site for subsequent site-saturation mutagenesis. This way, even mutants displaying inverted enantioselectivity compared to HheG wild type could be identified,[53–55] while the flexible *N*-terminal loop of HheG was not touched.
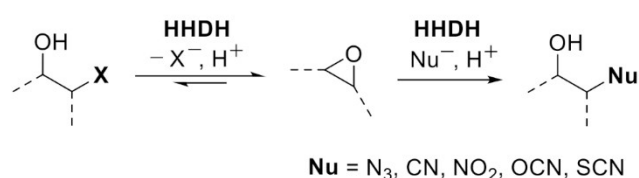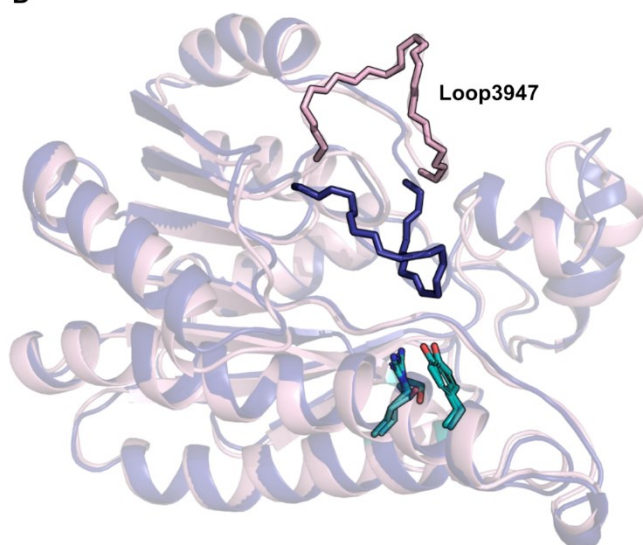
Figure 1. (**A**) HheG-catalyzed dehalogenation and epoxide ring opening reactions with small anionic nucleophiles. (**B**) Overlay of simulated structures of HheG monomer (PDB: 5o30) with either open (light pink) or closed (deepblue) conformation of loop3947. The catalytic residues of HheG (S152, Y165, R169) are highlighted in teal.

As our preliminary data hinted at a potential impact of the flexible loop covering residues T39 to G47 (in the following abbreviated loop3947) on the enantioselectivity of HheG, we surmised that highly enantioselective HheG variants could also be accessed through systematic engineering of this loop. To this end, two libraries containing defined single point mutants were generated and screened in ring opening reactions of chemically diverse epoxide substrates in

4

combination with different nucleophiles. This way, several HheG variants with largely increased or even inverted enantioselectivity as well as considerably improved activity towards the tested substrates could be identified.

RESULTS AND DISCUSSION

Loop engineering and library screening

Former approaches in our group to enhance the enantioselectivity of HheG in the ring opening of cyclic epoxides based on Rosetta analysis and active site mutagenesis only yielded single mutants with moderately increased enantioselectivity (e.g. HheG variant I104M achieved a product enantiomeric excess (ee$_P$) of 72% in the azidolysis of cyclohexene oxide (**1**), *unpublished data*), which is in agreement with data recently published by Tian et al.[54] As single point mutations on loop3947 of HheG turned out to influence the enantioselectivity of this enzyme as well, we shifted our focus to this loop for further protein engineering. To minimize our screening effort, positions T39 to G47 were initially only replaced by lysine, phenylalanine, cysteine and glutamate to incorporate a set of chemically diverse amino acids. Resulting HheG variants including wild type as well as a negative control (i.e. *E. coli* haboring an empty pET28a(+) vector) were produced in a 96-deep well plate yielding sufficient amounts of soluble enzyme (see Figure S1). This reduced library (in form of cell-free extract, CFE) was then screened in the azidolysis of cyclohexene oxide (**1**) (Scheme S1), achieving moderate to high conversions with all variants within 2 h of reaction (Figure 2A). Interestingly, the corresponding ee$_P$ values revealed that enantioselectivity of HheG was mainly affected by mutations at loop positions 44 to 46. Thus, nearly all tested variants at those three positions displayed improvements in enantioselectivity compared to HheG wild type (Figure 2B).[37,49,50] HheG M45F even formed azidoalcohol (1*S*,2*S*)-**2a** with a product enantiomeric excess of 96%.
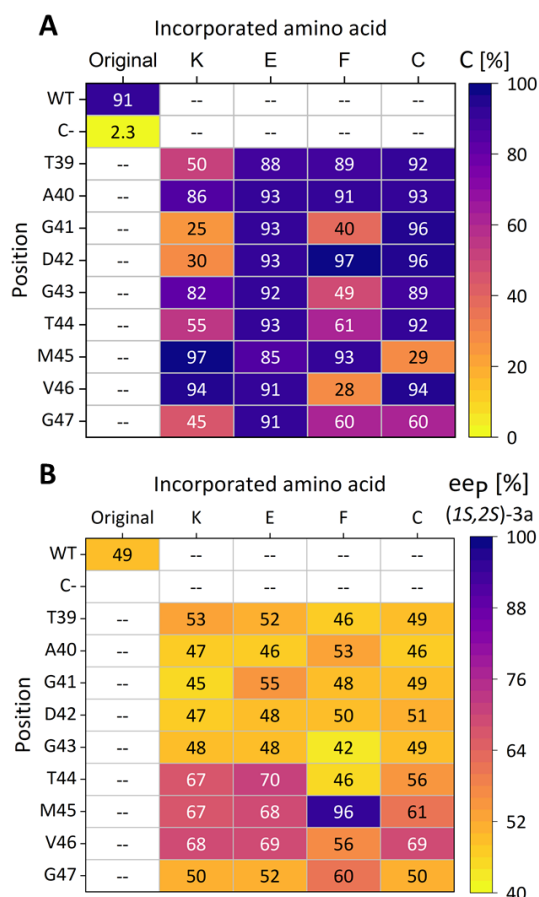
Figure 2. Screening result of a reduced library at loop3947 of HheG in the azidolysis of cyclohexene oxide (**1**). **A**: Conversion (C), **B**: product enantiomeric excess (ee$_P$). Reactions were performed at 22 °C and 900 rpm in 1 ml 50 mM Tris·SO$_4$, pH 7.0 using 200 μl cell-free extract (CFE), 20 mM cyclohexene oxide (**1**) and 40 mM sodium azide. Samples were taken after 2 h and analyzed by achiral and chiral GC.

As positions T44, M45 and V46 turned out to exert the highest impact on HheG selectivity, completely randomized libraries only on those positions were investigated next. To this end, all possible single variants were generated separately, produced in a 96-deep well plate and screened in the ring opening of cyclohexene oxide (**1**) with azide (again using CFE). Indeed, almost all variants displayed improved enantioselectivity compared to wild-type HheG (Figure 3), while conversion was always high (see Table S1 for absolute values). This result is in line with our reduced library data, confirming the importance of those three positions for HheG enantioselectivity. Interestingly, variants carrying an aromatic residue at position 45 yielded highest product enantiomeric excesses of 86% (M45Y), 92% (M45W) and 96% (M45F) (Table S1). This is striking as also aromatic residues at position 123 of HheG had the highest impact on the enzyme's stability and positively influenced enantioselectivity as well, presumably through regulation of the loop3947 dynamics.[37]
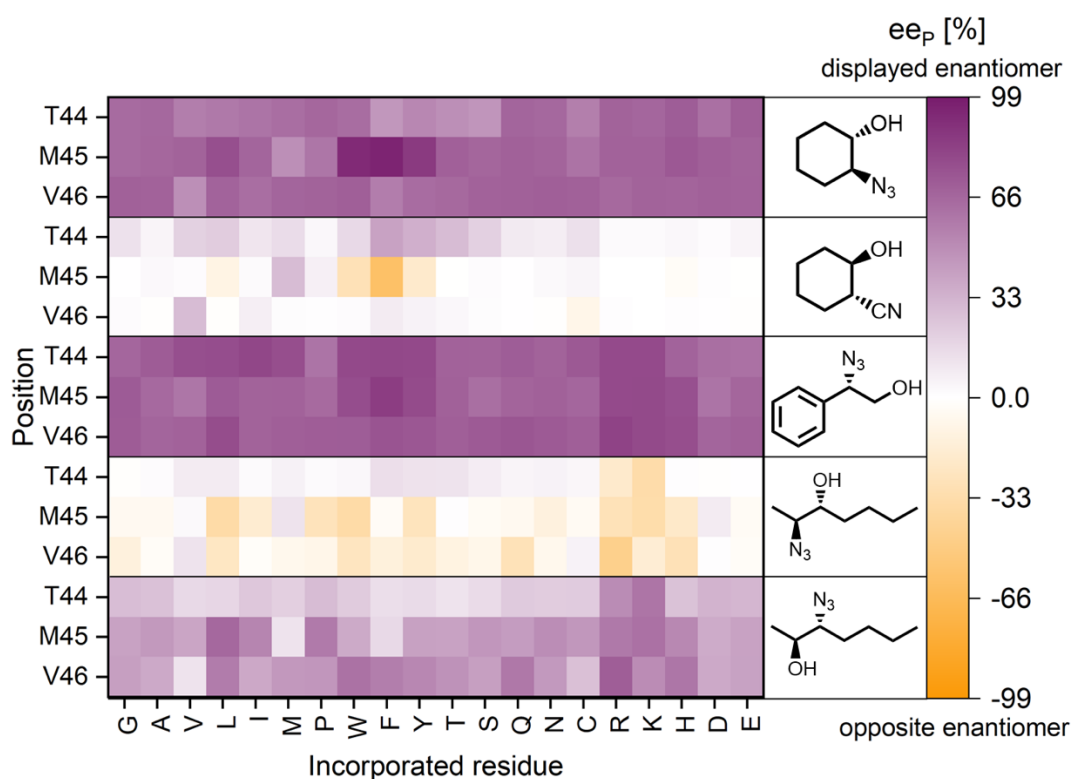
Figure 3. Screening result (product enantiomeric excess, ee$_P$) of the fully randomized library at positions 44, 45 and 46 of HheG in ring opening reactions of cyclohexene oxide (**1**), styrene oxide (**3**) and *trans*-2,3-heptene oxide (**5**) with azide as nucleophile as well as the ring opening of **1** with cyanide. Reactions were performed at 22 °C and 900 rpm in 1 ml 50 mM Tris·SO$_4$, pH 7.0 using either 100 µL (in reactions with **3** and **5**) or 200 µL CFE (in reactions with **1**), 10 or 20 mM epoxide (**1** and **3**: 20 mM; **5**: 10 mM) and 2 eq sodium azide or cyanide. Samples were taken after 2 h (azide) or 24 h (cyanide) for reactions with **1**, after 10 min in case of reactions with **3** and after 30 min for reactions with **5**. Samples were extracted and analyzed by achiral and chiral GC. Corresponding absolute ee$_P$ values as well as conversion data and E values are given in Tables S1-S6 in the supporting information.

To investigate whether this enantioselectivity improvement of HheG holds true for other reactions as well, the fully randomized library at positions 44 to 46 was further screened in the azidolysis of styrene oxide (**3**) and *trans*-2,3-heptene oxide (**5**) as well as the ring-opening of cyclohexene oxide (**1**) with cyanide (Scheme S1 and Figure 3). With cyanide as nucleophile, conversions of all HheG variants were much smaller compared to azide (Table S2), in agreement with previous reports.[42,47] Remarkably, variant M45F again displayed higher enantioselectivity, this time, however, for the opposite cyanoalcohol enantiomer compared to wild-type HheG[42], as well as a three-times higher conversion (Table S2). Also other aromatic residues at position 45 resulted in preferential formation of the (*1S,2R*)-product enantiomer, while HheG variants T44F and T44Y displayed slightly increased enantioselectivity compared to wild type for production of (*1R,2S*)-2-cyanocyclohexan-1-ol (Figure 3 and Table S2). Thus, an only minor difference in positioning of the aromatic residue on loop49[47] determines whether one or the other product enantiomer is formed, at least in the conversion of **1** with cyanide. Inversion in enantioselectivity upon loop engineering has also been reported for other HHDHs,

7

e.g. for HheC from *Agrobacterium radiobacter* AD1 and HheA from *Arthrobacter* sp. strain AD2 in the dehalogenation of 2-chloro-1-phenylethanol.[36][56] Both enzymes, however, do not possess such a highly flexible loop close to the N-terminus that would correspond to loop3947 of HheG.

With styrene oxide (**3**) as substrate, HheG preferentially catalyzes nucleophilic attack at the benzylic α-position (Scheme S1), which is the same as in the non-enzymatic reaction but opposite to the regioselectivity of most other HHDHs.[45] Thus, to preclude a reduction in product enantiomeric excess during azidolysis of **3** due to chemical background, screening reactions with **3** and azide were already stopped after 10 min, attaining between 50 and 60% of conversion (Table S3). This time, several loop variants displayed an increase in enantioselectivity with preferential formation of (*S*)-2-azidophenylethan-1-ol (**4**) like HheG wild type (Figure 3), while highest E-values of 40 and 46 were observed for variants carrying a phenylalanine at position 44 or 45, respectively, corresponding roughly to a two-fold improvement in comparison to wild-type HheG (Table S3). Hence, mutation M45F in HheG does not only impact the enzyme's enantioselectivity in the conversion of cyclohexene oxide, but also in the transformation of a structurally unrelated epoxide like styrene oxide.

Azidolysis of the internal epoxide **5** by HheG results in the formation of two different regioisomers, 2-azidoheptan-3-ol (**6a**) and 3-azidoheptan-2-ol (**6b**) (Scheme S1).[46] Both are roughly produced in equal amounts by wild-type HheG and this ratio did not significantly change upon loop engineering (Table S4). For several HheG variants, however, an inversion in enantiopreference compared to wild-type enzyme for formation of regioisomer **6a** could be observed (Figure 3), even though absolute E values were still quite low (highest E value of 2.8 for HheG V46R) (Table S5). In contrast, the enantiopreference of the loop variants in the formation of regioisomer **6b** was the same as for HheG wild type (Figure 3), but the enantioselectivity of many variants increased reaching ee_P values of up to 70% (for comparison, the ee_P of **6b** in the wild-type control was only 12%) (Table S6). This time, HheG variants T44K, M45L, M45K and V46R turned out to yield highest selectivity improvements, while HheG M45F displayed only minor changes in enantioselectivity compared to wild type (Figure 3 and Tables S5+S6).

In summary, screening of the fully randomized library at positions 44 to 46 with different substrates and nucleophiles always revealed several amino acid exchanges exerting a strong impact on HheG's enantioselectivity. This confirms our initial hypothesis that more selective HheG variants can indeed be accessed through engineering of loop3947. Moreover, only one mutation (M45F) on loop3947 was sufficient to obtain a highly selective HheG mutant for the azidolysis of cyclohexene oxide (**1**), giving azidoalcohol (1*S*,2*S*)-**2a** with 96%ee. In contrast, in the work by Tian et al.[54] based on the structure-guided mutagenesis of active-site residues of HheG, a triple mutant (Y18G/M189L/F200W) was necessary to obtain the same product enantiomer with 94%ee. This further emphasizes the importance of loop3947 for the enantioselectivity of HheG.

Characterization of beneficial variants

To further characterize the most beneficial HheG variants observed during screening, respective enzymes were produced on 100 mL scale and purified via immobilized metal ion affinity chromatography (IMAC). Subsequently, their specific activities and selectivities in respective

8

epoxide ring opening reactions, for which they had been identified during screening, as well as their apparent melting temperatures were determined (Table 1 and Table S7). Additionally, ring opening of **1** by HheG variants M45F, M45Y and M45W was also investigated using cyanate and nitrite, as HheG was recently shown to accept a broader range of nucleophiles.[47]

Table 1. Characterization data of purified HheG variants in epoxide ring opening reactions using different nucleophiles. Reactions were performed at 22 °C in 50 mM Tris·SO$_4$ buffer, pH 7.0 for the indicated amount of time and analyzed by achiral and chiral GC. All reactions were performed in duplicate.

Substrate	HheG variant	Conversion [%]		Product enantiomeric excess [%]		E value	
1 + N$_3^-$	WT	71 ± 0.2[a]		49 ± 0.4% (*1S,2S*)[a]		-	
	M45F	99 ± 0.1[a]		96 ± 0.8% (*1S,2S*)[a]		-	
	M45Y	97 ± 2.0[a]		86 ± 0.3% (*1S,2S*)[a]		-	
	M45W	79 ± 9.3[a]		91 ± 0.1% (*1S,2S*)[a]		-	
1 + CN$^-$	WT	20 ± 0.5%[b]		28 ± 0.0% (*1R,2S*)[b]		-	
	M45F	57 ± 0.3%[b]		60 ± 0.1% (*1S,2R*)[b]		-	
	M45Y	13 ± 1.4%[b]		19 ± 0.9% (*1S,2R*)[b]		-	
	M45W	10 ± 0.7%[b]		24 ± 0.9% (*1S,2R*)[b]		-	
1 + OCN$^-$	WT	54 ± 0.9%[b]		57 ± 0.3%[b,e]		-	
	M45F	95 ± 0.6%[b]		-40 ± 0.1%[b,e]		-	
	M45Y	18 ± 0.5%[b]		1.8 ± 0.0%[b,e]		-	
	M45W	7.2 ± 0.0%[b]		-30 ± 0.0%[b,e]		-	
1 + NO$_2^-$	WT	15 ± 0.1%[b] (73:27)[f]		0.1 ± 0.1%[b,e]		-	
	M45F	87 ± 0.0%[b] (60:40)[f]		44 ± 0.6%[b,e]		-	
	M45Y	10 ± 0.1%[b] (68:32)[f]		5.4 ± 0.3%[b,e]		-	
	M45W	9.3 ± 0.2%[b] (65:35)[f]		3.1 ± 0.3%[b,e]		-	
3 + N$_3^-$	WT	46 ± 1.4%[c]		84 ± 0.4% (*2S*)[c]		24 ± 1.9	
	T44F	53 ± 0.8%[c]		84 ± 1.0% (*2S*)[c]		44 ± 1.6	
	T44Y	53 ± 0.6%[c]		85 ± 0.4% (*2S*)[c]		42 ± 0.4	
	T44W	52 ± 0.8%[c]		82 ± 1.1% (*2S*)[c]		32 ± 0.4	
	M45F	52 ± 0.0%[c]		85 ± 0.1% (*2S*)[c]		39 ± 0.2	
5 + N$_3^-$		**6a**	**6b**	**6a**	**6b**	**6a**	**6b**
	WT	48 ± 0.1%[d]	51 ± 0.1%[d]	12 ± 0.3% (*2S,3R*)[d]	12 ± 0.0% (*2S,3R*)[d]	1.4 ± 0.0	1.4 ± 0.0
	T44K	36 ± 0.2%[d]	40 ± 0.1%[d]	4.7 ± 1.7% (*2R,3S*)[d]	38 ± 1.2% (*2S,3R*)[d]	1.1 ± 0.1	2.8 ± 0.1
	M45L	33 ± 0.4%[d]	45 ± 0.5%[d]	5.6 ± 0.6% (*2S,3R*)[d]	36 ± 0.6% (*2S,3R*)[d]	1.1 ± 0.0	2.8 ± 0.0
	M45K	25 ± 0.2%[d]	30 ± 0.2%[d]	29 ± 0.6% (*2R,3S*)[d]	61 ± 0.4% (*2S,3R*)[d]	2.0 ± 0.0	5.3 ± 0.1
	V46R	32 ± 1.0%[d]	36 ± 0.9%[d]	10 ± 2.8% (*2R,3S*)[d]	46 ± 1.9% (*2S,3R*)[d]	1.3 ± 0.1	3.5 ± 0.2

[a] determined after 2 h

[b] determined after 24 h

[c] determined after 10 min

[d] determined after 3 h

[e] enantiomers unassigned

[f] product ratio of nitroalcohol **2c**:diol **2f**

The resulting data do not only confirm the improvements in enantioselectivity observed during screening, but also highlight a concomitant increase in activity upon mutagenesis, which is especially evident for HheG M45F. This variant did not only achieve higher conversions compared to wild type in all studied epoxide ring opening reactions (Table 1), but displayed also an almost 10-fold higher specific activity in the azidolysis of **1** (Table S7), as determined by our recently published BTB assay.[57] Moreover, variant M45F was more than twice as active as HheG wild type in the ring opening of **3** with azide, while variant T44F exhibited the highest specific activity (Table S7) and the highest enantioselectivity (E=44, Table 1) in this reaction. Compared to other literature reports, this E value of 44 is not as high as that reported for other HHDHs, e.g. HheC[58] or HheA2 N178A,[36] that ─ unlike HheG ─ display β-regioselectivity in the ring opening of **3**. In contrast to most other HHDHs with α-regioselectivity,[13,59] however, all HheG variants preferentially convert (*R*)-styrene oxide yielding azidoalcohol (*S*)-**4** (Scheme S1).

When looking at the ring opening of epoxide **1** with cyanate and nitrite, the selectivity of variant M45F was again altered significantly in comparison to HheG wild type (Table 1). Using cyanate as nucleophile, M45F displayed an inverted enantioselectivity, as also observed with cyanide, while activity was increased as well. In the reaction with nitrite, only HheG variant M45F exhibited considerably enhanced selectivity and activity compared to HheG wild type, while the ratio of formed nitroalcohol:diol (**2c**:**2f**) was slightly affected for all tested variants (Table 1). Interestingly, HheG M45F was not only more active in epoxide ring opening reactions, but exhibited also a higher specific activity in the dehalogenation of 2-chlorocyclohexan-1-ol (**2e**) (0.07 U mg^{-1} for variant M45F compared to 0.02 U mg^{-1} for HheG wild type). Overall, our data using purified variants highlight that loop3947 in HheG does not only play a central role for the selectivity of HheG but also its activity. In contrast, the thermal stability of all tested variants seems to be hardly affected upon engineering of loop3947, as the determined apparent melting temperatures varied only slightly between the variants and HheG wild type (Table S7).

Regarding the ring opening of epoxide **5** with azide, the inversion in enantioselectivity for formation of regioisomer **6a** as well as the improvement in enantioselectivity for generation of regioisomer **6b** of the purified variants in comparison to wild-type HheG could be confirmed, while absolute E-values of the selected variants were lower compared to our initial screening results (Table 1). The latter is probably the result of the higher conversions (between 30 and 50%) that we aimed for in our reactions using purified enzymes in comparison to the screening. Based on these results, positions 44 to 46 on the loop are likely not the only relevant residues in HheG to steer the enzyme's enantioselectivity in the azidolysis of epoxide **5**.

To better understand why mutant M45F also displayed a tremendous increase in activity compared to HheG wild type, kinetic parameters of this variant in the azidolysis of cyclohexene oxide (**1**) were determined using our BTB assay (Table 2). This revealed not only a 5 to 15-fold increase in maximal reaction velocity ($k_{obs,max}$) of mutant M45F (rate improvement varies when either the kinetics for epoxide or azide are considered), but also a significant improvement in azide binding compared to HheG wild type. Interestingly, this loop mutation seems to enhance the cooperativity for azide binding, as the respective Hill coefficient n increased as well. A recent conformational landscape analysis of HheG demonstrated that loop3947 would affect

the presence and shape of substrate tunnel T3 in HheG.[51] The latter might impact nucleophile binding in HheG as well.

Table 2. Kinetic parameters of HheG wild type and mutant M45F in the azidolysis of cyclohexene oxide (**1**). First, the epoxide concentration was varied while keeping the azide concentration constant at 60 mM; afterwards, the azide concentration was varied while fixing the epoxide concentration at 100 mM. The Hill equation was used to fit the resulting data in OriginPro (Figure S2). Data for HheG wild type were taken from Staar et al. (2024),[57] as the exact same reaction conditions have been applied.

HheG variant	Cyclohexene oxide				Azide			
	K_{50} [mM]	$k_{obs,max}$ [s^{-1}]	$k_{obs,max}/K_{50}$ [s^{-1} mM^{-1}]	n [-]	K_{50} [mM]	$k_{obs,max}$ [s^{-1}]	$k_{obs,max}/K_{50}$ [s^{-1} mM^{-1}]	n [-]
wild type[57]	39.4 ±2.69	2.31 ±0.15	0.06 ±0.01	3.81 ±0.78	38.4 ±2.09	4.12 ±0.15	0.11 ±0.01	2.92 ±0.36
M45F	28.0 ±0.64	31.1 ±0.39	1.11 ±0.03	3.33 ±0.27	10.1 ±0.21	20.2 ±0.26	1.99 ±0.01	3.94 ±0.29

Computational analyses

Intrigued by how mutation M45F enhances HheG's activity and enantioselectivity towards the epoxide-ring opening reaction of cyclohexene oxide (**1**) with azide, we decided to computationally evaluate HheG wild type and mutant M45F by means of Molecular Dynamics (MD) simulations in the presence and absence of substrates. M45F is contained in loop3947, whose conformational dynamics regulate the formation of the available tunnels for substrate binding and product release.[51] Our study therefore first focused on the comparison of the conformational dynamics of HheG wild type and variant M45F (Figure 4A). We performed 5 replicas of 250 ns MD simulations (1.25 µs per system in tetrameric conformation) for both systems in (i) the absence of any ligand, and (ii) with both azide and epoxide **1** bound in the active site (see Experimental section for computational details). We performed Principal Component Analysis (PCA) considering the pairwise distances between the heavy atoms of residues included in loop3947 and the rest of the residues of the protein. The reconstructed free energy landscapes (FELs) indicate that wild type and M45F adopt two different conformations of loop3947: a closed ($\mathbf{C^{OUT}}$) conformation in which the sidechain of residue M/F45 points outside the active site, and an open conformation presenting M/F45 inside of the pocket ($\mathbf{O^{IN}}$, see Figure 4A, B). The estimated FELs suggest that in the absence of any ligand wild type mostly adopts the $\mathbf{C^{OUT}}$ conformation of loop3947, whereas in the case of M45F both conformations are visited, being $\mathbf{O^{IN}}$ the most stable minima. This different $\mathbf{C^{OUT}}/\mathbf{O^{IN}}$ conformation of loop3947 has a large impact on the available tunnels for substrate binding and product release. As shown in Figure 4B, the closed conformation of loop3947 favors the formation of tunnels named T1, previously found to be present in most HHDHs, and T2, which is mostly found in HheG and HheC.[51] The open conformation of loop3947 with the sidechain of M/F45 in the active site blocks the formation of tunnel 2 (T2), but instead opens tunnel 3 (T3) that is mostly observed in G-type HHDHs (Figures 4B, S3 and Table S10).[51] The analysis of the conformational landscape and available tunnels for HheG wild type and variant M45F suggests that the introduced mutation favors the exploration of both open and closed

11

conformations of loop3947, which affects T2/T3 formation potentially impacting the productive binding of both substrates in the active site pocket.

The MD simulations performed in the presence of both substrates indicate that in wild-type HheG the side chain of M45 is highly flexible, which affects the positioning of the epoxide and azide in the active site. As shown in Figure 4C, azide can be either retained in the nucleophile binding site (grey region in Figure 4C) or get displaced close to the catalytic serine (teal region in Figure 4C), which hampers the epoxide-ring opening reaction. The introduction of mutation M45F favors the produtive binding of cyclohexene oxide (**1**) in the active site by establishing non-covalent C-H $\cdots\pi$ interactions with F45 (Figure S4). At the same time, azide is preferentially bound at the nucleophile binding pocket (grey region in Figure 4C). These simulations therefore indicate that mutation M45F helps retaining both the epoxide and azide in a catalytically competent pose in the active site pocket, which is in line with the lower K_{50} for azide and the higher $k_{obs,max}$ observed experimentally (Table 2).

To estimate the differences in enantioselectivity, we performed Quantum Mechanics (QM) *theozyme* calculations to determine the ideal distances and angles for the azide-mediated cyclohexene oxide ring-opening reaction and evaluated the number of MD frames displaying a pro-*S*/pro-*R* conformation. QM calculations indicate that at the transition state the nucleophilic attack distance is 2.2 Å with an N_{azide}-N_{azide}-$C_{(1)}$ angle of ca. 109º, whereas in the reactant complex the distance is 3.2 Å and the angle 85º (Figure S5). We filtered the number of MD frames presenting catalytically competent poses by considering distances < 4 Å between the epoxide oxygen of **1** and the catalytic Tyr165, as well as the distance (< 4 Å) and angle (range of 80 to 120º) between azide and either C_1/C_2 of cyclohexene oxide corresponding to pro-*S*/pro-*R* attacks, respectively (see Figure S5). Using this filtering scheme, we could get an estimation of the enantiomeric excess, which our simulations predict to be 13.7 % and 40.7 % for wild type and variant M45F, respectively. These simulations therefore suggest that mutation M45F restricts the flexibility of position 45 by establishing non-covalent C-H$\cdots\pi$ interactions with the epoxide. This interaction observed in M45F helps retaining the substrate and azide in the active site and promotes the enantioselective epoxide-ring opening reaction by positioning C_1 closer to the azide for the selective formation of the (1*S*,2*S*)-product.
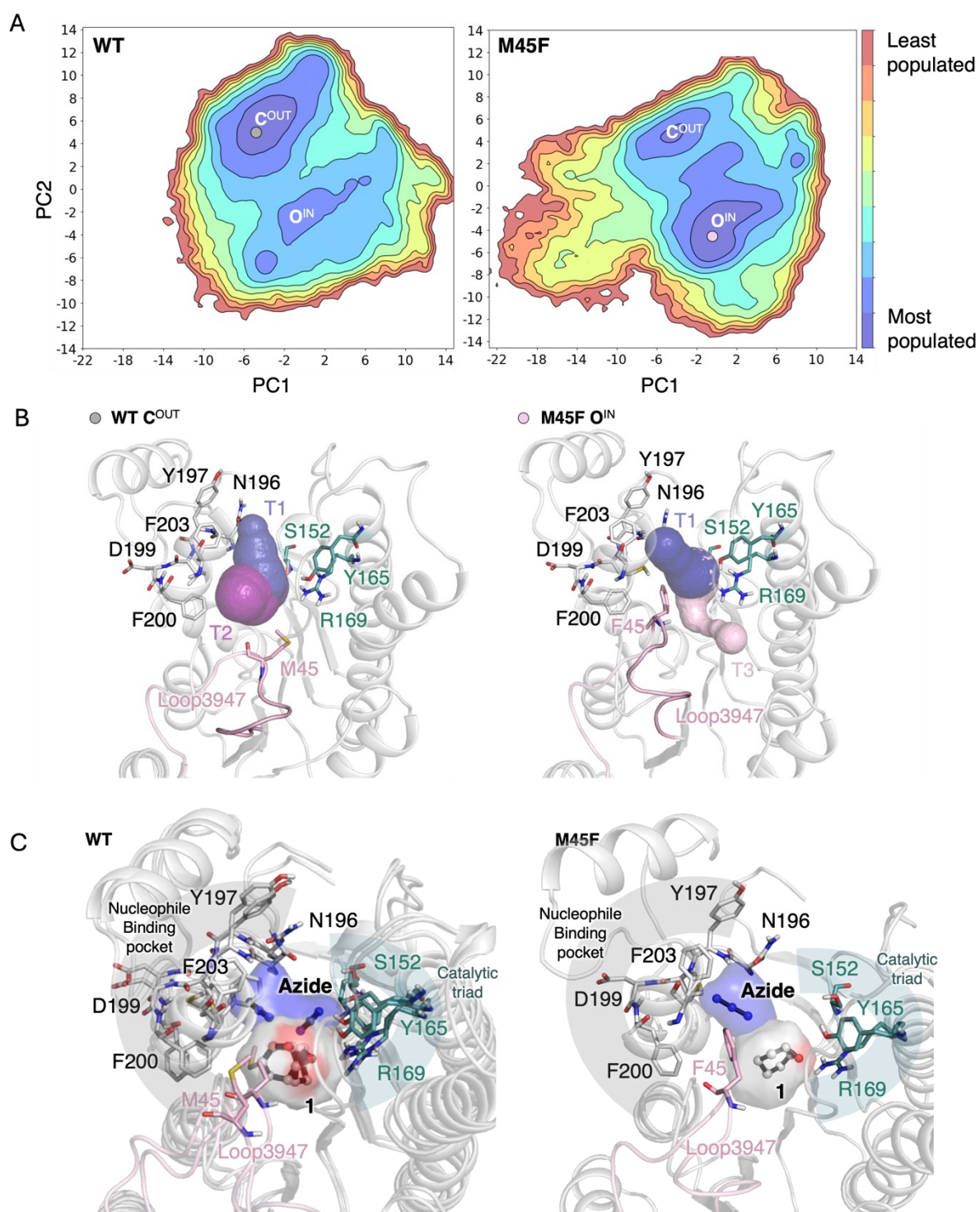
Figure 4. A Estimated free energy landscapes (FEL) of HheG wild type (WT) and variant M45F in the absence of any substrate. PC1 and PC2 describe the open/closed conformational change of loop3947 and the sidechain orientation of M/F45 within the active site pocket. Most stable conformations are colored in blue, whereas least stable ones in red. **B** A representative structure of the most populated minima is displayed together with the available tunnels: $\mathbf{C}^{OUT}$ conformation for wild type (WT) presenting the loop closed and the sidechain of M45 outside the active site pocket, and $\mathbf{O}^{IN}$ of variant M45F in which loop3947 is closed and F45 accommodated in the active site. Tunnel 1 (T1) is shown in dark blue, whereas tunnel 2 (T2) in

13

purple and tunnel 3 (T3) in light pink. **C** Representative structures of HheG wild type (WT) and variant M45F taken from the MD simulations performed in the presence of both cyclohexene oxide (**1**) and azide. For WT, two different conformations of the protein are overlaid. A surface representation containing all poses of **1** and azide sampled is displayed. Cyclohexene oxide (**1**) and especially azide can adopt multiple conformations in the active site pocket of HheG wild type, in line with its inferior catalytic activity. Nucleophile binding site residues are shown using gray sticks, catalytic residues in teal, and loop3947 and position 45 in light pink. Cyclohexene oxide (**1**) and azide are represented using spheres and black sticks.

Combinatorial mutagenesis and loop deletion

As our studied loop3947 variants of HheG did not exhibit sufficient thermal stability while being improved in terms of activity and selectivity, promising variants from this study, namely M45F, M45Y and M45W, were subsequently combined with mutations at position 123 of HheG. Previously, we reported that aromatic amino acids as well as glycine at position 123 resulted in significantly thermostable HheG variants.[37] Moreover, some of these variants, especially T123F and T123G, displayed enhanced activity as well. Based on crystal structure analysis and MD simulations, a possible interaction between positions M45 and T123 was hypothesized.[37] Thus, respective double mutants were generated using site-directed mutagenesis, produced, purified and tested in reactions with the same epoxides and nucleophiles as used for our single mutants before. As desired, resulting double mutants of HheG exhibited higher apparent melting temperatures (up to 12 K increase) in comparison to wild-type HheG (Table S7). Additionally, some double mutants were even further improved in terms of activity. Thus, variant M45F-T123G displayed an almost 2 times higher specific activity (14.6 U mg^{-1}) in the azidolysis of **3** compared to the best single variant T44F (Table S7). Likewise, this variant achieved also much higher conversions in the ring opening of **1** with cyanide (93% after 24 h) and cyanate (99% after 24 h, Table S8) in comparison to HheG M45F (see Table 1). Apart from that, enantioselectivity of the loop variants was generally not further improved by combination with mutations at position 123 (Table S8). Interestingly, however, the selectivity of some double mutants for formation of nitroalcohol **2c** in comparison to diol **2f** in the ring opening of **1** with nitrite was decreased (Table S8).

Furthermore, HheG variants lacking either the complete loop3947 or parts of it were investigated to gain further insights regarding the impact of this loop on HheG performance. To this end, three defined variants were generated: HheG Del39-47 with complete deletion of loop3947, HheG Del44-46 where only residues T44, M45 and V46 were eliminated, and HheG Ins-DPAE in which loop3947 was replaced by a short linker containing residues aspartate, proline, alanine and glutamate. This short sequence is present at the corresponding position of loop3947 in an HheG homolog from *Actinomycetota bacterium* (the same protein was also reported from *Acidimicrobiia bacterium*) that was recently described.[13,60] Deletion of all residues from position 39 to 47 resulted in complete inactivation of HheG, even though soluble, and thus folded, enzyme could still be obtained (data not shown). In contrast, elimination of residues T44, M45, V46 (HheG Del44-46) as well as exchange of loop3947 with the short linker sequence (HheG Ins-DPAE) yielded active variants displaying significantly increased specific

14

activity in the azidolysis of **3** compared to wild-type HheG, while the activity in the ring opening of **1** was generally reduced (Table S7). The enantioselectivity of both variants was also altered compared to HheG wild type, but no general trend could be observed (Table S9). Interestingly, both deletion variants again formed (1*S*,2*R*)-**2b** with slight preference in the cyanolysis of **1**, which is the opposite enantiomer to that formed by HheG wild type preferentially. This further underlines the importance of loop3947 for regulation of HheG's activity and enantioselectivity, probably through differences in substrate und nucleophile positioning within the active site. Remarkably, complete deletion of loop3947 (as in HheG Del39-47) considerably decreased enzyme stability as well, as evident from a decrease in apparent melting temperature (T_m) by 5 K in comparison to wild-type HheG. In contrast, corresponding T_m values of deletion variants Del44-47 and Ins-DPAE were only slightly reduced (Table S7).

Construction of a stable and enantioselective biocatalyst

Recently, we reported the efficient immobilization of HheG (especially variant D114C) in the form of cross-linked enzyme crystals (CLECs),[49,50] which yielded an HheG preparation displaying high process stability as well as easy operability in different chemical reactor systems (batch and continuous flow).[61] Thus, we herein aimed to combine mutation M45F with D114C with the goal to prepare enantioselective HheG CLECs. The resulting double mutant HheG M45F-D114C could be obtained in high yield (231 mg L^{-1} in comparison to 140 mg L^{-1} for HheG M45F) and displayed a similar specific activity in the azidolysis of **1** (18.3 U mg^{-1}) as HheG M45F (16.5 U mg^{-1}). Crystallization of this double mutant using the optimized crystallization conditions of HheG D114C led to hexagonal-shaped crystals after 24 h (Figure S6). Cross-linking with BMOE yielded stable HheG M45F-D114C CLECs that achieved 92% conversion in the ring opening of 20 mM **1** with azide already after 1 h and a high product enantiomeric excess (ee$_P$) of 95% (in comparison to 82% conversion and 49%ee$_P$ using wild-type HheG; Figure S7). Therefore, respective CLECs were subsequently applied in a semi-preparative reaction using 50 mM cyclohexene oxide (**1**) and 2 eq azide in 10 mL scale. After 2 h, full conversion was reached and (1*S*,2*S*)-2-azidocyclohexan-1-ol (**2a**) was obtained in 74% isolated yield (52 mg) with an ee$_P$ of 96%. This demonstrates that HheG variant M45F can be stabilized successfully via CLEC formation yielding a stable and highly enantioselective HheG preparation for future application in repetitive batch and continous flow.

CONCLUSION

Overall, we have demonstrated that loop3947 is highly important for regulating the activity as well as enantioselectivity of HheG. In this context, variant M45F was identified displaying greatly increased activity and improved enantioselectivity in the ring opening of cyclohexene oxide with various nucleophiles. Likewise, HheG T44F displayed the highest activity and enantioselectivity increase in the azidolysis of styrene oxide among the screened loop3947 variants. In contrast, complete deletion of this dynamic loop resulted in soluble but inactive enzyme. This highlights the significance of loop3947 for catalytic performance of HheG. As close homologs of HheG, which have recently been described by us,[47] feature comparable loops, a similar impact of loop mutations on their catalytic performance can be expected. Hence, future protein enginering campaigns of HheG or its homologs to improve or alter activity and

enantioselectivity should not only focus on active-site mutations but include loop variations as well.

In addition, by combining the enantioselectivity-conferring mutation M45F with mutation D114C, which facilitates to immobilize HheG as CLECs, a stable biocatalyst was created exhibiting also improved activity and enantioselectivity. This does not only enhance the industrial applicability of HheG M45F, but further demonstrates that our previously published approach of HheG CLEC formation can be expanded to other HheG variants.

EXPERIMENTAL SECTION

Chemicals

Substrates cyclohexene oxide (**1**) and styrene oxide (**3**) as well as crosslinker bis-maleimidoethane (BMOE) were purchased from Thermo Fisher Scientific (Geel, Belgium). Substrate *trans*-2,3-heptene-oxide (**5**) was synthesized according to Calderini et al.[41] starting from *trans*-2-heptene. Substrate 2-chlorocyclohexanol (**2e**) was purchased from TCI (Tokyo, Japan). All commercial chemicals were of highest available purity.

Bacterial strains and plasmids

E. coli BL21(DE3) Gold was used for cloning as well as heterologous protein production as described previously.[21] Further, expression vector pET-28a(+) (Merck) was used to carry respective mutant genes under control of the T7 promoter, resulting in the addition of an N-terminal His$_6$-tag to heterologously produced proteins.

HheG enigneering

Protein engineering of HheG with the aim to increase its enantioselectivity focussed on the exchange of residues on loop3947. In a first step positions T39 to G47 were exchanged by amino acids Cys, Lys, Glu and Phe. Site-directed mutagenesis of HheG was performed using the PfuUltra II Hotstart PCR Mastermix (Agilent Technologies, Santa-Clara, CA, United States). Respective forward and reverse mutagenic primers (Table S11) were designed with PrimerX (Carlo Lapid, 2003, http://bioinformatics.org/primerx/index.htm, accessed on 16 February 2021), purchased from Merck (Darmstadt, Germany) and used in concentrations of 0.25 µM each with 100 ng of pET28a(+)-*hheG* template.[37] Otherwise, the PCR protocol for mutagenesis was in agreement with the manufacturer's instructions. Afterwards, methylated parental DNA was digested at 37 °C over night using 20 U DpnI before transformation in *E. coli* BL21(DE3) Gold.

In a second step, positions T44, M45 and V46 were fully randomized. GoldenGate cloning[62] was used to incorporate all missing mutations at respective positions separately. The PCR using Q5 polymerase (NEB) was performed according to the manufacturer's instructions. Forward and reverse mutagenic primers (Table S11) were designed according to GoldenGate primer design,[62] purchased from Merck (Darmstadt, Germany) and used in concentrations of 0.25 µM each with 5 ng of pET28a(+)-*hheG* template. Each 100 ng PCR product were purified using the E.Z.N.A. MircoElute CyclePure Kit (omega-biotek) and incubated with 2 U BsaI plus 200 U T4-Ligase in 1x CutSmart buffer and 1x T4-ligase buffer for 2 h at 30 °C. Inactivated GoldenGate reactions (20 min, 65 °C) were afterwards transformed in *E. coli* BL21(DE3) Gold. For combination of mutations M45F, M45Y and M45W with previously described mutations T123G and T123F of HheG,[37] site-directed mutagenesis or GoldenGate cloning was performed according to the protocols described above and using templates pET28a(+)-*hheG T123G* and pET28a(+)-*hheG T123F*. For combination of mutations M45F and D114C in HheG, site-directed mutagenesis starting from template pET28a(+)-*hheG D114C* was used. Loop3947 deletion mutants of HheG were constructed by GoldenGate cloning using pET28a(+)-*hheG* as template and mutagenic primers listed in Table S11.

Protein production and purification

Protein production in 96-well format

For library expression in 96-deep-well plates (HJ Bioanalytik, Erkelenz, Germany), each 1 mL teriffic broth (TB) medium (per liter: 4 mL glycerol, 12 g peptone, 24 g yeast extract, 0.17 M KH_2PO_4, 0.74 M K_2HPO_4) supplemented with 50 µg mL^{-1} kanamycine and 0.2 mM isopropyl-β-thiogalactopyranosid (IPTG) was inoculated with 10% (v/v) overnight pre-culture. Protein production was carried out at room temperature and 1050 rpm for 24 h. Cells were harvested by centrifugation (3494 g, 20 min, 4 °C) and cell pellets were stored in the deep-well plate at -20 °C until further use.

Cell lysis was performed by freezing and thawing cycles. Frozen cell pellets were resuspended in each 300 µl Tris·SO_4 buffer, pH 7.0 supplemented with 1 mg mL^{-1} lysozyme and 1 pierce protease inhibitor tablet (Thermo Fisher Scientific) per 10 mL. The cell suspension was incubated at 30 °C and 700 rpm for 1 h before freezing at -20 °C for 30 min. The cell suspension was thawed again and incubated for another 1 h at 30 °C and 700 rpm. After the first 30 min, 50 µL DNaseI-solution (0.1 mg mL^{-1} DNase in 20 mM $MgSO_4$) was added. Afterwards, the suspension was centrifuged (3494 g, 60 min, 4 °C) and the resulting cell free extract (CFE) was used for library screening.

Protein production in 100 mL scale and purification via gravity-flow

Selected HheG variants displaying improved enantioselectivity during screening as well as loop3947 deletion variants were produced in shaking flasks containing 100 mL TB medium supplemented with 50 µg mL^{-1} kanamycine and 0.2 mM IPTG. After inoculation with 10% (v/v) pre-culture, protein production was performed for 24 h at 22 °C and 220 rpm. Cells were harvested by centrifugation (3494 g, 20 min, 4 °C) and resulting cell pellets were stored at -20 °C until further use.

For subsequent IMAC-based purification using gravity-flow columns, cells were resuspended in 20 mL lysis buffer (50 mM Tris·SO_4 buffer, pH 7.9, 25 mM imidazole) supplemented with 1 mg mL^{-1} lysozyme and 1 pierce protease inhibitor tablet. Sonification was perfomed on ice (65% amplitude, 10 s pulse, 20 s pause). Cell debris was removed by centrifugation (18000 g, 45 min, 4 °C) and the resulting CFE was filtered through a 0.45 µm filter. Protein purification was performed using pierce gravity-flow columns (Thermo Fisher Scientific) containing 2 mL Ni-NTA sepharose (Cytiva, Freiburg, Germany). The column material was first equilibrated with 10 column volumes (CV) lysis buffer. The CFE was loaded on the column. After flow through, the column was washed with 10 CV lysis buffer. For elution of desired proteins, 10 CV elution buffer (50 mM Tris·SO_4 buffer, pH 7.9, 500 mM imidazole) were used. The first 2.5 mL of elution containing the desired protein were collected and desalted using PD10 desalting columns in combination with TE buffer (10 mM Tris·SO_4 buffer, pH 7.9, 4 mM ethylenediamine tetraacetic acid, 10% (v/v) glycerol) according to the manufacturer's instructions. Desalted proteins were stored at -20 °C until further use. Protein concentrations were determined by measuring the absorbance at 280 nm using an NP80 nanophotometer (Implen, München, Germany) and calculated via the Lambert-Beer law with molar extinction coefficients and molecular weights of the respective proteins obtained from Protparam[63].

Protein production in 500 mL scale and purification via FPLC

For kinetic analysis of HheG M45F as well as crystallization of HheG M45F-D114C, both variants were produced in 500 mL scale according to the protocol described above, and purified via their N-terminal His-tag using fast protein liquid chromatography (FPLC). Cell disruption was performed as described above but using 30 mL buffer A (50 mM Tris·SO$_4$, 300 mM Na$_2$SO$_4$, 25 mM imidazole, pH 7.9), supplemented with 1 mg mL^{-1} lysozyme and 1 Pierce Protease Inhibitor Mini Tablet, for cell resuspension. Cell free extracts were loaded with a flow rate of 2 mL min^{-1} on a 5 mL HisTrap FF column (GE Healthcare, Freiburg, Germany), pre-equilibrated with lysis buffer, using an ÄktaStart FPLC system (GE Healthcare). Afterwards, the column was washed with 10 CV of buffer A to remove other proteins. His-tagged protein was eluted using a gradient over 60 mL to 100% buffer B (50 mM Tris·SO$_4$, 300 mM Na$_2$SO$_4$, 500 mM imidazole, pH 7.9) while collecting 1 mL fractions. Fractions with highest UV absorbance were pooled and desalted using a HiPrep 26/10 desalting column (GE Healthcare), pre-equilibrated with TE buffer (10 mM Tris·SO$_4$, 4 mM EDTA, pH 7.9, 10% (v/v) glycerol). During desalting, protein was eluted using TE buffer. Desalted protein fractions with highest UV absorbance were concentrated using Vivaspin Turbo 15 centrifugation units (Sartorius, Göttingen, Germany) with 10 kDa molecular weight cut-off. Protein concentrations of resulting purified protein solutions were determined as described above. Both HheG variants were stored at -20 °C until further use.

Library screening

Library screening with different epoxides and nucleophiles was performed in glas vials using each 1 mL 50 mM Tris·SO$_4$ buffer, pH 7.0 containing 200 µL CFE (100 µL in case of styrene oxide **3**) of respective library variants as well as 20 mM epoxide (10 mM in case of *trans*-2,3-heptene oxide **5**) and 2 eq of nucleophile at 22 °C and 900 rpm. Samples were taken at different time points (2 and 24 h with epoxide **1** + azide and haloalcohol **2e**; 24 h with epoxide **1**+ cyanide; 10 min with epoxide **3** + azide; 30 min with epoxide **5**+azide) and extracted with an equal volume of *tert*-buthylmethylether (TBME) containing 0.1% dodecane as internal standard. Organic phases were dried over MgSO$_4$ and analyzed via achiral (conversion of **1** and **5**) and chiral GC (enantiomeric excesses as well as conversion of **3**). Temperature programs and retention times of substrates and products are listed in Table S12.

Protein crystallization and cross-linking

Crystallization and cross-linking of HheG variant M45F-D114C was performed as described before for variant D114C in 200 µL scale.[49] In a vial, 100 µL of a 24 mg mL^{-1} protein solution were mixed with 100 µL crystallization buffer (10 mM HEPES, pH 7.0, 8% (w/v) PEG4000) and incubated for 24 h at 8 °C. The resulting crystals were collected by centrifugation for 3 min at 400 *g* and cross-linked for 24 h at 8 °C with 2 mM bis-maleimidoethane (ThermoFisher Scientific) dissvoled in crystallization buffer containing 10% (v/v) dimethylsulfoxide. After cross-linking, CLECs were collected by centrifugation, washed with 200 µL 50 mM Tris·SO$_4$, pH 7.0, and centrifuged again. Obtained CLECs were resuspended in 50 mM Tris·SO$_4$ buffer, pH 7.0 to a concentration of 2 mg mL^{-1}. Microscopic analysis of the CLECs was performed using microscope SMZ-171-TLED (Moticeurope, Barcelona, Spain).

Biocatalysis using purified enzymes

Biocatalytic reactions using purified enzymes (HheG wild type and selected variants) were performed under the same reaction conditions as described for library screening but using 5 to 400 µg mL^{-1} of purified enzyme. Samples were taken after specific time points (2 h for epoxide **1** + azide; 24 h for epoxide **1** + cyanide, cyanate and nitrite; 10 min for epoxide **3** + azide; 30 min for epoxide **5** + azide), extracted with an equal volume of TBME containing 0.1% dodecane as internal standard and analyzed by achiral and chiral GC (Table S12). Time points were selected to minimize chemical background reactions. All reactions were performed in duplicate. E values were calculated according to Chen et al.[64]

Reactions to compare soluble HheG wild-type and soluble variant M45F-D114C with CLECs of HheG M45F-D114C were performed in 1 mL 50 mM Tris·SO$_4$ buffer, pH 7.0 containing 20 mM cyclohexene oxide (**1**), 40 mM azide and 200 µg biocatalyst. Reactions were incubated for 1 h at 22 °C and 900 rpm. Reactions were performed in duplicate, extracted with an equal volume of TBME containing 0.1% dodecane as internal standard and analyzed by achiral and chiral GC (Table S12).

Preparative-scale reaction

A preparative scale reaction using CLECs of HheG M45-D114C was performed in 10 mL 50 mM Tris·SO$_4$ buffer, pH 7.0 containing 50 mM cyclohexene oxide (**1**), 100 mM azide and 2 mg CLECs. The reaction was stirred for 2 h at room temperature and 800 rpm. Afterwards, the reaction mixture was extracted once with 10 mL TBME, the organic fraction was dried over anhydrous MgSO$_4$ and the solvent was removed by evaporation yielding the product as yellowish oil[65]. The product was further analyzed by achiral and chiral GC (Table S12).

Thermal shift assay

Apparent melting temperatures (T_m) of purified HheG variants were determine by thermal shift assay according to a previously described protocol.[49] Each measurement contained 10 µg biocatalyst and 5x SYPRO orange fluorescent dye in TE buffer in a total of 50 µL volume.

BTB assay

Specific activities of HheG variants in epoxide ring opening reactions were determined by bromothymolblue (BTB) assay as described previously.[57] Reactions were performed in 1 mL 2 mM MOPS buffer, pH 7.0 containing 20 mM epoxide (only 10 mM in case of epoxide **5**), 2 eq azide and 5-500 µg enzyme. Samples were taken within 4 min for styrene oxide (**3**), within 6 min for *trans*-2,3-heptene oxide (**5**) and within 15 min for cyclohexene oxide (**1**). Each 100 µL sample was mixed with an equal volume of 40 µg mL^{-1} BTB dissolved in 100 % (v/v) methanol in 96-well microtiter plates (Sarstedt, Nümbrecht, Germany), and analyzed regarding absorbance at 499 and 616 nm using a CLARIOstar plate reader (BMG Labtech, Ortenberg, Germany). The subsequent calculation of consumed protons and resulting activities was performed as described previously.[57]

The BTB assay was also used to determine kinetic parameters of HheG variant M45F in epoxide ring opening of cyclohexene oxide (**1**) with azide based on initial reaction velocities. General reaction conditions were the same as for specific activity determination, but only 10 µg HheG M45F were applied. First, the concentration of epoxide **1** was varied (5, 10, 20, 25, 30, 40, 50,

60, 80, 90, 100, 110, 120, 130, 140 and 150 mM) while keeping the azide concentration constant at 60 mM. Afterwards, the azide concentration was varied (1, 2.5, 5, 7.5, 10, 15, 20, 40, 60, 80, 100 mM) while keeping the cyclohexene oxide (**1**) concentration constant at 100 mM. Reactions were performed in duplicate. To determine initial reaction velocities, each 100 μL samples were taken after 30, 60, 90 and 120 s. Resulting activities [in μmol min^{-1}] were calculated as described previously,[57] plotted over the applied substrate concentration and fitted in OriginPro 2021 using a Hill fit.

Halide release assay

Specific activities of selected HheG variants (wild type and M45F) in the dehalogenation of 2-chlorocyclohexanol (**2e**) were determined by halide release assay as described previously.[26] Reactions were performed in 1 mL 25 mM Tris·SO$_4$ buffer, pH 7.0 containing 20 mM **2e** and 400 μg biocatalyst at 22 °C. Samples were taken after 30, 80, 180, 270 and 360 s. Specific activities were calculated based on released halide ions. Reactions were performed in duplicate. Chemical background dehalogenation in reactions without enzyme addition was substracted.

MD simulations

Parameters for substrates **1** and azide were generated with the antechamber and parmchk2 modules of AMBER20[66] using the 2nd generation of the general amber force-field (GAFF2).[67,68] Partial charges (RESP model)[69] were set to fit the electrostatic potential generated at the HF/6-31G(d) level of theory. The charges were calculated according to the Merz-Singh-Kollman[70,71] scheme using the Gaussian16 software package.[72] The protonation states were predicted using PROPKA.[73,74] The enzyme structure was obtained from the PDB with the code 5o30[42] and cleaned from other non-peptidic molecules to obtain the wild-type system in a tetrameric oligomerization state. The single mutation M45F was introduced using the Pymol mutagenesis tool. Proteins were solvated in a pre-equilibrated truncated octahedral box of 12 Å edge distance using the OPC water model, resulting in the addition of *ca.* 21.300 water molecules, and neutralized by the addition of explicit counterions (*i.e.*, Na$^+$) using the AMBER20 leap module. All MD simulations were performed using the amber19 force field (ff19SB)[75] in our in-house GPU cluster, GALATEA.

The Pmemd.cuda program from Amber20 was used to perform a two-stage geometry optimization. In the first stage, solvent molecules and ions were minimized, while solute molecules were restrained using 500 kcal·mol^{-1}·Å^{-2} harmonic positional restraints. In the second stage, an unrestrained minimization was performed. The systems were then gradually heated by increasing the temperature by 50 K during six 20 ps sequential MD simulations (0–300 K) under constant volume. Harmonic restraints of 10 kcal·mol^{-1}·Å^{-2} were applied to the solute, and the Langevin equilibration scheme was used to control and equalize the temperature. The time step was kept at one fs during the heating stages to allow potential inhomogeneities to self-adjust. Each system was then equilibrated without restraints for 2 ns at a constant pressure of 1 atm and temperature of 300 K using a 2 fs time step in the isothermal-isobaric ensemble (NPT). After equilibration, five replicas of 250 ns were run for each system (*i.e.*, 1.25 μs per system and 5 μs in total simulated time) in the canonical ensemble (NVT). MD simulations were analyzed by monomers to make it easier to study, multiplying the simulated

time by four. All analysis was done using available Python libraries (pyemma[76], mdtraj[77], and mdanalysis[78]) in a jupyter lab environment.

QM calculations

Geometry minimizations were performed using Gaussian16[72], using the hybrid density functional theory method B3LYP[79,80] including dispersion corrections, and the 6-31G+(d,p) basis set. Solvation effects were considered using the SMD solvation model, a variation of Truhlar's and coworkers' integral equation formalism variant (IEFPCM)[81], using diethyl ether as solvent.

AUTHOR INFORMATION

Corresponding author

*Anett Schallmey, E-mail: a.schallmey@tu-braunschweig.de

*Sílvia Osuna, E-mail: silviaosu@gmail.com

Notes

The authors declare no competing interests.

ACKNOWLEDGEMENT

REFERENCES

(1)   Ritzen, B.; van Oers, M. C. M.; van Delft, F. L.; Rutjes, F. P. J. T. Enantioselective Chemoenzymatic Synthesis of Trans-Aziridines. *J. Org. Chem.* **2009**, *74* (19), 7548–7551. https://doi.org/10.1021/jo901548t.

(2)   Schubert, T.; Hummel, W.; Kula, M.-R.; Müller, M. Enantioselective Synthesis of Both Enantiomers of Various Propargylic Alcohols by Use of Two Oxidoreductases. *Eur. J. Org. Chem.* **2001**, *2001* (22), 4181–4187. https://doi.org/10.1002/1099-0690(200111)2001:22<4181::AID-EJOC4181>3.0.CO;2-T.

(3)   Takabe, K.; Iida, Y.; Hiyoshi, H.; Ono, M.; Hirose, Y.; Fukui, Y.; Yoda, H.; Mase, N. Reverse Enantioselectivity in the Lipase-Catalyzed Desymmetrization of Prochiral 2-Carbamoylmethyl-1,3-Propanediol Derivatives. *Tetrahedron Asymmetry* **2000**, *11* (24), 4825–4829. https://doi.org/10.1016/S0957-4166(00)00473-0.

(4)   Kerridge, A.; Willetts, A.; Holland, H. Stereoselective Oxidation of Sulfides by Cloned Naphthalene Dioxygenase. *J. Mol. Catal. B Enzym.* **1999**, *6* (1), 59–65. https://doi.org/10.1016/S1381-1177(98)00121-0.

(5)   Koszelewski, D.; Tauber, K.; Faber, K.; Kroutil, W. ω-Transaminases for the Synthesis of Non-Racemic α-Chiral Primary Amines. *Trends Biotechnol.* **2010**, *28* (6), 324–332. https://doi.org/10.1016/j.tibtech.2010.03.003.

(6) Reetz, M. T. Controlling the Enantioselectivity of Enzymes by Directed Evolution: Practical and Theoretical Ramifications. *Proc. Natl. Acad. Sci.* **2004**, *101* (16), 5716–5722. https://doi.org/10.1073/pnas.0306866101.

(7) Qiao, L.; Luo, Z.; Chen, H.; Zhang, P.; Wang, A.; Sheldon, R. A. Engineering Ketoreductases for the Enantioselective Synthesis of Chiral Alcohols. *Chem. Commun.* **2023**, *59* (49), 7518–7533. https://doi.org/10.1039/D3CC01474F.

(8) Song, Z.; Zhang, Q.; Wu, W.; Pu, Z.; Yu, H. Rational Design of Enzyme Activity and Enantioselectivity. *Front. Bioeng. Biotechnol.* **2023**, *11*. https://doi.org/10.3389/fbioe.2023.1129149

(9) Maldonado, M. R.; Alnoch, R. C.; de Almeida, J. M.; Santos, L. A. dos; Andretta, A. T.; Ropaín, R. del P. C.; de Souza, E. M.; Mitchell, D. A.; Krieger, N. Key Mutation Sites for Improvement of the Enantioselectivity of Lipases through Protein Engineering. *Biochem. Eng. J.* **2021**, *172*, 108047. https://doi.org/10.1016/j.bej.2021.108047.

(10) Findrik Blažević, Z.; Milčić, N.; Sudar, M.; Majerić Elenkov, M. Halohydrin Dehalogenases and Their Potential in Industrial Application – A Viewpoint of Enzyme Reaction Engineering. *Adv. Synth. Catal.* **2021**, *363* (2), 388–410. https://doi.org/10.1002/adsc.202000984.

(11) Janssen, D. B.; Dinkla, I. J. T.; Poelarends, G. J.; Terpstra, P. Bacterial Degradation of Xenobiotic Compounds: Evolution and Distribution of Novel Enzyme Activities. *Environ. Microbiol.* **2005**, *7* (12), 1868–1882. https://doi.org/10.1111/j.1462-2920.2005.00966.x.

(12) Hasnaoui-Dijoux, G.; Majerić Elenkov, M.; Spelberg, J. H. L.; Hauer, B.; Janssen, D. B. Catalytic Promiscuity of Halohydrin Dehalogenase and Its Application in Enantioselective Epoxide Ring Opening. *ChemBioChem* **2008**, *9* (7), 1048–1051. https://doi.org/10.1002/cbic.200700734.

(13) Wang, H.-H.; Wan, N.-W.; Miao, R.-P.; He, C.-L.; Chen, Y.-Z.; Liu, Z.-Q.; Zheng, Y.-G. Identification and Structure Analysis of an Unusual Halohydrin Dehalogenase for Highly Chemo-, Regio- and Enantioselective Bio-Nitration of Epoxides. *Angew. Chem. Int. Ed.* **2022**, *61* (37), e202205790. https://doi.org/10.1002/anie.202205790.

(14) Schrittwieser, J. H.; Lavandera, I.; Seisser, B.; Mautner, B.; Kroutil, W. Biocatalytic Cascade for the Synthesis of Enantiopure β-Azidoalcohols and β-Hydroxynitriles. *Eur. J. Org. Chem.* **2009**, *2009* (14), 2293–2298. https://doi.org/10.1002/ejoc.200900091.

(15) Majerić Elenkov, M. M.; Tang, L.; Meetsma, A.; Hauer, B.; Janssen, D. B. Formation of Enantiopure 5-Substituted Oxazolidinones through Enzyme-Catalysed Kinetic Resolution of Epoxides. *Org. Lett.* **2008**, *10* (12), 2417–2420. https://doi.org/10.1021/ol800698t.

(16) Ma, R.; Hua, X.; He, C.-L.; Wang, H.-H.; Wang, Z.-X.; Cui, B.-D.; Han, W.-Y.; Chen, Y.-Z.; Wan, N.-W. Biocatalytic Thionation of Epoxides for Enantioselective Synthesis of Thiiranes. *Angew. Chem. Int. Ed.* **2022**, *61* (52), e202212589. https://doi.org/10.1002/anie.202212589.

(17) Lutje Spelberg, J. H.; van Hylckama Vlieg, J. E. T.; Bosma, T.; Kellogg, R. M.; Janssen, D. B. A Tandem Enzyme Reaction to Produce Optically Active Halohydrins, Epoxides and Diols. *Tetrahedron Asymmetry* **1999**, *10* (15), 2863–2870. https://doi.org/10.1016/S0957-4166(99)00308-0.

(18) Lutje Spelberg, J. H.; van Hylckama Vlieg, J. E. T.; Tang, L.; Janssen, D. B.; Kellogg, R. M. Highly Enantioselective and Regioselective Biocatalytic Azidolysis of Aromatic Epoxides. *Org. Lett.* **2001**, *3* (1), 41–43. https://doi.org/10.1021/ol0067540.

(19) Majerić Elenkov, M.; Hoeffken, H. W.; Tang, L.; Hauer, B.; Janssen, D. B. Enzyme-Catalyzed Nucleophilic Ring Opening of Epoxides for the Preparation of Enantiopure Tertiary Alcohols. *Adv. Synth. Catal.* **2007**, *349* (14–15), 2279–2285. https://doi.org/10.1002/adsc.200700146.

(20) Majerić Elenkov, M.; Primožič, I.; Hrenar, T.; Smolko, A.; Dokli, I.; Salopek-Sondi, B.; Tang, L. Catalytic Activity of Halohydrin Dehalogenases towards Spiroepoxides. *Org. Biomol. Chem.* **2012**, *10* (26), 5063–5072. https://doi.org/10.1039/C2OB25470K.

(21) Schallmey, M.; Koopmeiners, J.; Wells, E.; Wardenga, R.; Schallmey, A. Expanding the Halohydrin Dehalogenase Enzyme Family: Identification of Novel Enzymes by Database Mining. *Appl. Environ. Microbiol.* **2014**, *80* (23), 7303–7315. https://doi.org/10.1128/AEM.01985-14.

(22) Xue, F.; Yu, X.; Shang, Y.; Peng, C.; Zhang, L.; Xu, Q.; Li, A. Heterologous Overexpression of a Novel Halohydrin Dehalogenase from Pseudomonas Pohangensis and Modification of Its

Enantioselectivity by Semi-Rational Protein Engineering. *Int. J. Biol. Macromol.* **2020**, *146*, 80–88. https://doi.org/10.1016/j.ijbiomac.2019.12.203.

(23) Xue, F.; Ya, X.; Tong, Q.; Xiu, Y.; Huang, H. Heterologous Overexpression of Pseudomonas Umsongensis Halohydrin Dehalogenase in Escherichia Coli and Its Application in Epoxide Asymmetric Ring Opening Reactions. *Process Biochem.* **2018**, *75*, 139–145. https://doi.org/10.1016/j.procbio.2018.09.018.

(24) Xue, F.; Ya, X.; Xiu, Y.; Tong, Q.; Wang, Y.; Zhu, X.; Huang, H. Exploring the Biocatalytic Scope of a Novel Enantioselective Halohydrin Dehalogenase from an Alphaproteobacterium. *Catal. Lett.* **2019**, *149* (2), 629–637. https://doi.org/10.1007/s10562-019-02659-0.

(25) Lutje Spelberg, J. H.; Tang, L.; Kellogg, R. M.; Janssen, D. B. Enzymatic Dynamic Kinetic Resolution of Epihalohydrins. *Tetrahedron Asymmetry* **2004**, *15* (7), 1095–1102. https://doi.org/10.1016/j.tetasy.2004.02.009.

(26) Koopmeiners, J.; Halmschlag, B.; Schallmey, M.; Schallmey, A. Biochemical and Biocatalytic Characterization of 17 Novel Halohydrin Dehalogenases. *Appl. Microbiol. Biotechnol.* **2016**, *100* (17), 7517–7527. https://doi.org/10.1007/s00253-016-7493-9.

(27) Wan, N.-W.; Liu, Z.-Q.; Xue, F.; Shen, Z.-Y.; Zheng, Y.-G. A One-Step Biocatalytic Process for (S)-4-Chloro-3-Hydroxybutyronitrile Using Halohydrin Dehalogenase: A Chiral Building Block for Atorvastatin. *ChemCatChem* **2015**, *7* (16), 2446–2450. https://doi.org/10.1002/cctc.201500453.

(28) Majerić Elenkov, M.; Hoeffken, H. W.; Tang, L.; Hauer, B.; Janssen, D. B. Enzyme-Catalyzed Nucleophilic Ring Opening of Epoxides for the Preparation of Enantiopure Tertiary Alcohols. *Adv. Synth. Catal.* **2007**, *349* (14–15), 2279–2285. https://doi.org/10.1002/adsc.200700146.

(29) Mehić, E.; Hok, L.; Wang, Q.; Dokli, I.; Miklenić, M. S.; Blažević, Z. F.; Tang, L.; Vianello, R.; Elenkov, M. M. Expanding the Scope of Enantioselective Halohydrin Dehalogenases – Group B. *Adv. Synth. Catal.* **2022**, *364* (15), 2576–2588. https://doi.org/10.1002/adsc.202200342.

(30) Yu, F.; Nakamura, T.; Mizunashi, W.; Watanabe, I. Cloning of Two Halohydrin Hydrogen-Halide-Lyase Genes of Corynebacterium Sp. Strain N-1074 and Structural Comparison of the Genes and Gene Products. *Biosci. Biotechnol. Biochem.* **1994**, *58* (8), 1451–1457. https://doi.org/10.1271/bbb.58.1451.

(31) Van Den Wijngaard, A. J.; Janssen, D. B.; Witholt, B. 1989. Degradation of Epichlorohydrin and Halohydrins by Bacterial Cultures Isolated from Freshwater Sediment. *Microbiology* **1989**, *135* (8), 2199–2208. https://doi.org/10.1099/00221287-135-8-2199.

(32) Schallmey, M.; Jekel, P.; Tang, L.; Majerić Elenkov, M.; Höffken, H. W.; Hauer, B.; Janssen, D. B. A Single Point Mutation Enhances Hydroxynitrile Synthesis by Halohydrin Dehalogenase. *Enzyme Microb. Technol.* **2015**, *70*, 50–57. https://doi.org/10.1016/j.enzmictec.2014.12.009.

(33) Tang, L.; van Merode, A. E. J.; Lutje Spelberg, J. H.; Fraaije, M. W.; Janssen, D. B. Steady-State Kinetics and Tryptophan Fluorescence Properties of Halohydrin Dehalogenase from Agrobacterium Radiobacter. Roles of W139 and W249 in the Active Site and Halide-Induced Conformational Change. *Biochemistry* **2003**, *42* (47), 14057–14065. https://doi.org/10.1021/bi034941a.

(34) Wang, H.-H.; Wan, N.-W.; Da, X.-Y.; Mou, X.-Q.; Wang, Z.-X.; Chen, Y.-Z.; Liu, Z.-Q.; Zheng, Y.-G. Enantiocomplementary Synthesis of β-Adrenergic Blocker Precursors via Biocatalytic Nitration of Phenyl Glycidyl Ethers. *Bioorganic Chem.* **2023**, 106640. https://doi.org/10.1016/j.bioorg.2023.106640.

(35) Fox, R. J.; Davis, S. C.; Mundorff, E. C.; Newman, L. M.; Gavrilovic, V.; Ma, S. K.; Chung, L. M.; Ching, C.; Tam, S.; Muley, S.; Grate, J.; Gruber, J.; Whitman, J. C.; Sheldon, R. A.; Huisman, G. W. Improving Catalytic Function by ProSAR-Driven Enzyme Evolution. *Nat. Biotechnol.* **2007**, *25* (3), 338–344. https://doi.org/10.1038/nbt1286.

(36) Tang, L.; Zhu, X.; Zheng, H.; Jiang, R.; Majerić Elenkov, M. Key Residues for Controlling Enantioselectivity of Halohydrin Dehalogenase from Arthrobacter Sp. Strain AD2, Revealed by Structure-Guided Directed Evolution. *Appl. Environ. Microbiol.* **2012**, *78* (8), 2631–2637. https://doi.org/10.1128/AEM.06586-11.

(37) Solarczek, J.; Klünemann, T.; Brandt, F.; Schrepfer, P.; Wolter, M.; Jacob, C. R.; Blankenfeldt, W.; Schallmey, A. Position 123 of Halohydrin Dehalogenase HheG Plays an Important Role in Stability, Activity, and Enantioselectivity. *Sci. Rep.* **2019**, *9* (1), 5106. https://doi.org/10.1038/s41598-019-41498-2.

(38) Tang, X.-L.; Ye, G.-Y.; Wan, X.-Y.; Li, H.-W.; Zheng, R.-C.; Zheng, Y.-G. Rational Design of Halohydrin Dehalogenase for Efficient Chiral Epichlorohydrin Production with High Activity and Enantioselectivity in Aqueous-Organic Two-Phase System. *Biochem. Eng. J.* **2020**, *161*, 107708. https://doi.org/10.1016/j.bej.2020.107708.

(39) Wang, X.; Han, S.; Yang, Z.; Tang, L. Improvement of the Thermostability and Activity of Halohydrin Dehalogenase from Agrobacterium Radiobacter AD1 by Engineering C-Terminal Amino Acids. *J. Biotechnol.* **2015**, *212*, 92–98. https://doi.org/10.1016/j.jbiotec.2015.08.013.

(40) de Jong, R. M.; Tiesinga, J. J. W.; Rozeboom, H. J.; Kalk, K. H.; Tang, L.; Janssen, D. B.; Dijkstra, B. W. Structure and Mechanism of a Bacterial Haloalcohol Dehalogenase: A New Variation of the Short-Chain Dehydrogenase/Reductase Fold without an NAD(P)H Binding Site. *EMBO J.* **2003**, *22* (19), 4933–4944. https://doi.org/10.1093/emboj/cdg479.

(41) Wessel, J.; Petrillo, G.; Estevez-Gay, M.; Bosch, S.; Seeger, M.; Dijkman, W. P.; Iglesias-Fernández, J.; Hidalgo, A.; Uson, I.; Osuna, S.; Schallmey, A. Insights into the Molecular Determinants of Thermal Stability in Halohydrin Dehalogenase HheD2. *FEBS J.* **2021**, *288* (15), 4683–4701. https://doi.org/10.1111/febs.15777.

(42) Koopmeiners, J.; Diederich, C.; Solarczek, J.; Voß, H.; Mayer, J.; Blankenfeldt, W.; Schallmey, A. HheG, a Halohydrin Dehalogenase with Activity on Cyclic Epoxides. *ACS Catal.* **2017**, *7* (10), 6877–6886. https://doi.org/10.1021/acscatal.7b01854.

(43) Watanabe, F.; Yu, F.; Ohtaki, A.; Yamanaka, Y.; Noguchi, K.; Yohda, M.; Odaka, M. Crystal Structures of Halohydrin Hydrogen-Halide-Lyases from Corynebacterium Sp. N-1074. *Proteins Struct. Funct. Bioinforma.* **2015**, *83* (12), 2230–2239. https://doi.org/10.1002/prot.24938.

(44) de Jong, R. M.; Kalk, K. H.; Tang, L.; Janssen, D. B.; Dijkstra, B. W. The X-Ray Structure of the Haloalcohol Dehalogenase HheA from Arthrobacter Sp. Strain AD2: Insight into Enantioselectivity and Halide Binding in the Haloalcohol Dehalogenase Family. *J. Bacteriol.* **2006**, *188* (11), 4051–4056. https://doi.org/10.1128/JB.01866-05.

(45) An, M.; Liu, W.; Zhou, X.; Ma, R.; Wang, H.; Cui, B.; Han, W.; Wan, N.; Chen, Y. Highly α-Position Regioselective Ring-Opening of Epoxides Catalyzed by Halohydrin Dehalogenase from Ilumatobacter Coccineus : A Biocatalytic Approach to 2-Azido-2-Aryl-1-Ols. *RSC Adv.* **2019**, *9* (29), 16418–16422. https://doi.org/10.1039/C9RA03774H.

(46) Calderini, E.; Wessel, J.; Süss, P.; Schrepfer, P.; Wardenga, R.; Schallmey, A. Selective Ring-Opening of Di-Substituted Epoxides Catalysed by Halohydrin Dehalogenases. *ChemCatChem* **2019**, *11* (8), 2099–2106. https://doi.org/10.1002/cctc.201900103.

(47) Solarczek, J.; Kaspar, F.; Bauer, P.; Schallmey, A. G-Type Halohydrin Dehalogenases Catalyze Ring Opening Reactions of Cyclic Epoxides with Diverse Anionic Nucleophiles. *Chem. – Eur. J.* **2022**, *28* (72), e202202343. https://doi.org/10.1002/chem.202202343.

(48) Zhou, C.; Chen, X.; Lv, T.; Han, X.; Feng, J.; Liu, W.; Wu, Q.; Zhu, D. Flipping the Substrate Creates a Highly Selective Halohydrin Dehalogenase for the Synthesis of Chiral 4-Aryl-2-Oxazolidinones from Readily Available Epoxides. *ACS Catal.* **2023**, 4768–4777. https://doi.org/10.1021/acscatal.2c06417.

(49) Staar, M.; Henke, S.; Blankenfeldt, W.; Schallmey, A. Biocatalytically Active and Stable Cross-Linked Enzyme Crystals of Halohydrin Dehalogenase HheG by Protein Engineering. *ChemCatChem* **2022**, *14* (9), e202200145. https://doi.org/10.1002/cctc.202200145.

(50) Staar, M.; Staar, S.; Schallmey, A. Crystal Contact Engineering for Enhanced Cross-Linking Efficiency of HheG Crystals. *Catalysts* **2022**, *12* (12), 1553. https://doi.org/10.3390/catal12121553.

(51) Estévez-Gay, M.; Iglesias-Fernández, J.; Osuna, S. Conformational Landscapes of Halohydrin Dehalogenases and Their Accessible Active Site Tunnels. *Catalysts* **2020**, *10* (12), 1403. https://doi.org/10.3390/catal10121403.

(52) Ma, J.-M.; Wang, Y.-F.; Miao, R.-P.; Jin, X.; Wang, H.-H.; Chen, Y.-Z.; Wan, N.-W. Biocatalytic Construction of Spiro-Oxazolidinones via Halohydrin Dehalogenase-Catalyzed Ring Expansion of Spiro-Epoxides. *ACS Catal.* **2024**, *14* (14), 10670–10678. https://doi.org/10.1021/acscatal.4c02122.

(53) Song, J.; Zhou, C.; Chen, X.; Gu, Y.; Xue, F.; Wu, Q.; Zhu, D. Engineering of Halohydrin Dehalogenases for the Regio- and Stereoselective Synthesis of (S)-4-Aryl-2-Oxazolidinones. *Catal. Sci. Technol.* **2024**, *14* (7), 1967–1976. https://doi.org/10.1039/D3CY01584J.

(54) Tian, S.; Ge, X.; Yan, Q.; Li, M.; Huang, Q.; Zhang, X.; Ma, M.; Chen, B.; Wang, J. Directed Evolution of Stereoselective Enzymes Meets Click Reactions: Asymmetric Synthesis of Chiral Triazoles Using a Cu(I)-Compatible Halohydrin Dehalogenase. *Green Synth. Catal.* **2024**. https://doi.org/10.1016/j.gresc.2024.01.001.

(55) Zhou, X.-Y.; Wang, Y.-F.; Fu, H.-K.; Wang, H.-H.; Chen, Y.-Z.; Wan, N.-W. Biocatalytic Regio- and Enantiocomplementary Synthesis of Chiral Aryloxazolidinones. *Adv. Synth. Catal.* **2024**, *366* (11), 2461–2467. https://doi.org/10.1002/adsc.202400169.

(56) Guo, C.; Chen, Y.; Zheng, Y.; Zhang, W.; Tao, Y.; Feng, J.; Tang, L. Exploring the Enantioselective Mechanism of Halohydrin Dehalogenase from Agrobacterium Radiobacter AD1 by Iterative Saturation Mutagenesis. *Appl. Environ. Microbiol.* **2015**, *81* (8), 2919–2926. https://doi.org/10.1128/AEM.04153-14.

(57) Staar, S.; Estévez-Gay, M.; Kaspar, F.; Osuna, S.; Schallmey, A. Engineering of Conserved Sequence Motif 1 Residues in Halohydrin Dehalogenase HheC Simultaneously Enhances Activity, Stability and Enantioselectivity. *ChemRxiv* **2024**. https://doi.org/10.26434/chemrxiv-2024-cw4cm.

(58) Lutje Spelberg, J. H.; van Hylckama Vlieg, J. E. T.; Tang, L.; Janssen, D. B.; Kellogg, R. M. Highly Enantioselective and Regioselective Biocatalytic Azidolysis of Aromatic Epoxides. *Org. Lett.* **2001**, *3* (1), 41–43. https://doi.org/10.1021/ol0067540.

(59) Zhou, C.; Chen, X.; Lv, T.; Han, X.; Feng, J.; Liu, W.; Wu, Q.; Zhu, D. Flipping the Substrate Creates a Highly Selective Halohydrin Dehalogenase for the Synthesis of Chiral 4-Aryl-2-Oxazolidinones from Readily Available Epoxides. *ACS Catal.* **2023**, 4768–4777. https://doi.org/10.1021/acscatal.2c06417.

(60) Günther, S.; Schallmey, A. Characterization of a New G-Type Halohydrin Dehalogenase with Enhanced Catalytic Activity. *ChemRxiv* **2022**. https://doi.org/10.26434/chemrxiv-2022-p9rzx.

(61) Staar, M.; Schallmey, A. Performance of Cross-Linked Enzyme Crystals of Engineered Halohydrin Dehalogenase HheG in Different Chemical Reactor Systems. *Biotechnol. Bioeng.* **2023**, *120* (11), 3210–3223. https://doi.org/10.1002/bit.28528.

(62) Engler, C.; Kandzia, R.; Marillonnet, S. A One Pot, One Step, Precision Cloning Method with High Throughput Capability. *PLoS ONE* **2008**, *3* (11). https://doi.org/10.1371/journal.pone.0003647.

(63) Gasteiger, E.; Hoogland, C.; Gattiker, A.; Duvaud, S.; Wilkins, M. R.; Appel, R. D.; Bairoch, A. Protein Identification and Analysis Tools on the ExPASy Server. In *The Proteomics Protocols Handbook*; Walker, J. M., Ed.; Springer Protocols Handbooks; Humana Press: Totowa, NJ, 2005; pp 571–607. https://doi.org/10.1385/1-59259-890-0:571.

(64) Chen, C. S.; Fujimoto, Y.; Girdaukas, G.; Sih, C. J. Quantitative Analyses of Biochemical Kinetic Resolutions of Enantiomers. *J. Am. Chem. Soc.* **1982**, *104* (25), 7294–7299. https://doi.org/10.1021/ja00389a064.

(65) Christoffers, J.; Schulze, Y.; Pickardt, J. Synthesis, Resolution, and Absolute Configuration of Trans-1-Amino-2-Dimethylaminocyclohexane. *Tetrahedron* **2001**, *57* (9), 1765–1769. https://doi.org/10.1016/S0040-4020(00)01172-8.

(66) Case, D. A.; KB, I.; Ben-Shalom, S. R.; Brozell, D. S.; Cerutti III, T. E.; Cheatham III, V. W. D.; Cruzeiro, T. A.; Darden, R. E.; Duke, G. G.; Gilson, M. K. DMY and PAK Amber 2020. *Univ. Calif. San Franc.* **2020**.

(67) Wang, J.; Wolf, R. M.; Caldwell, J. W.; Kollman, P. A.; Case, D. A. Development and Testing of a General Amber Force Field. *J. Comput. Chem.* **2004**, *25* (9), 1157–1174. https://doi.org/10.1002/jcc.20035.

(68) Case, D. A.; Cerutti, D.; Cheateham, T.; Darden, T.; Duke, R.; Giese, T.; Gohlke, H.; Goetz, A. W.; Greene, D.; Homeyer, N. AMBER16 Package. *Univ. Calif. San Franc. CA USA* **2016**.

(69) Bayly, C. I.; Cieplak, P.; Cornell, W.; Kollman, P. A. A Well-Behaved Electrostatic Potential Based Method Using Charge Restraints for Deriving Atomic Charges: The RESP Model. *J. Phys. Chem.* **1993**, *97* (40), 10269–10280. https://doi.org/10.1021/j100142a004.

(70) Singh, U. C.; Kollman, P. A. An Approach to Computing Electrostatic Charges for Molecules. *J. Comput. Chem.* **1984**, *5* (2), 129–145. https://doi.org/10.1002/jcc.540050204.

(71) Besler, B. H.; Merz Jr., K. M.; Kollman, P. A. Atomic Charges Derived from Semiempirical Methods. *J. Comput. Chem.* **1990**, *11* (4), 431–439. https://doi.org/10.1002/jcc.540110404.

(72) Frisch, M. ea; Trucks, G. W.; Schlegel, H. B.; Scuseria, G. E.; Robb, M. A.; Cheeseman, J. R.; Scalmani, G.; Barone, V.; Petersson, G. A.; Nakatsuji, H. *Gaussian 16, Revision C. 01*; Gaussian, Inc., Wallingford CT, 2016.

(73) Olsson, M. H. M.; Søndergaard, C. R.; Rostkowski, M.; Jensen, J. H. PROPKA3: Consistent Treatment of Internal and Surface Residues in Empirical PKa Predictions. *J. Chem. Theory Comput.* **2011**, *7* (2), 525–537. https://doi.org/10.1021/ct100578z.

(74) Søndergaard, C. R.; Olsson, M. H. M.; Rostkowski, M.; Jensen, J. H. Improved Treatment of Ligands and Coupling Effects in Empirical Calculation and Rationalization of PKa Values. *J. Chem. Theory Comput.* **2011**, *7* (7), 2284–2295. https://doi.org/10.1021/ct200133y.

(75) Tian, C.; Kasavajhala, K.; Belfon, K. A. A.; Raguette, L.; Huang, H.; Migues, A. N.; Bickel, J.; Wang, Y.; Pincay, J.; Wu, Q.; Simmerling, C. Ff19SB: Amino-Acid-Specific Protein Backbone Parameters Trained against Quantum Mechanics Energy Surfaces in Solution. *J. Chem. Theory Comput.* **2020**, *16* (1), 528–552. https://doi.org/10.1021/acs.jctc.9b00591.

(76) Scherer, M. K.; Trendelkamp-Schroer, B.; Paul, F.; Pérez-Hernández, G.; Hoffmann, M.; Plattner, N.; Wehmeyer, C.; Prinz, J.-H.; Noé, F. PyEMMA 2: A Software Package for Estimation, Validation, and Analysis of Markov Models. *J. Chem. Theory Comput.* **2015**, *11* (11), 5525–5542. https://doi.org/10.1021/acs.jctc.5b00743.

(77) McGibbon, R. T.; Beauchamp, K. A.; Harrigan, M. P.; Klein, C.; Swails, J. M.; Hernández, C. X.; Schwantes, C. R.; Wang, L.-P.; Lane, T. J.; Pande, V. S. MDTraj: A Modern Open Library for the Analysis of Molecular Dynamics Trajectories. *Biophys. J.* **2015**, *109* (8), 1528–1532. https://doi.org/10.1016/j.bpj.2015.08.015.

(78) Gowers, R. J.; Linke, M.; Barnoud, J.; Reddy, T. J. E.; Melo, M. N.; Seyler, S. L.; Domański, J.; Dotson, D. L.; Buchoux, S.; Kenney, I. M.; Beckstein, O. MDAnalysis: A Python Package for the Rapid Analysis of Molecular Dynamics Simulations. *Proc. 15th Python Sci. Conf.* **2016**, 98–105. https://doi.org/10.25080/Majora-629e541a-00e.

(79) Becke, A. D. Density-functional Thermochemistry. I. The Effect of the Exchange-only Gradient Correction. *J. Chem. Phys.* **1992**, *96* (3), 2155–2160. https://doi.org/10.1063/1.462066.

(80) Stephens, P. J.; Devlin, F. J.; Chabalowski, C. F.; Frisch, M. J. Ab Initio Calculation of Vibrational Absorption and Circular Dichroism Spectra Using Density Functional Force Fields. *J. Phys. Chem.* **1994**, *98* (45), 11623–11627. https://doi.org/10.1021/j100096a001

(81) Marenich, A. V.; Cramer, C. J.; Truhlar, D. G. Universal Solvation Model Based on Solute Electron Density and on a Continuum Model of the Solvent Defined by the Bulk Dielectric Constant and Atomic Surface Tensions. *J. Phys. Chem. B* **2009**, *113* (18), 6378–6396. https://doi.org/10.1021/jp810292n.